Design guidelines for thermopower generators with multi-layered black phosphorus

Parijat Sengupta
Dept. of Electrical Engineering
University of Illinois at Chicago
Chicago, IL, 60607, USA

Giftsondass Irudayadass
Dept. of Electrical Engineering
University of Illinois at Chicago
Chicago, IL, 60607, USA

Junxia Shi
Dept. of Electrical Engineering
University of Illinois at Chicago
Chicago, IL, 60607, USA

***Abstract*—We study a thermal gradient induced current (I_{th}) flow in potassium (*K*)-doped two-dimensional anisotropic black phosphorus (BP) with semi-Dirac dispersion. The prototype device is a BP channel clamped between two contacts maintained at unequal temperatures. The choice of BP lies in the predicted efficient thermolectric behaviour. A temperature-induced difference in the Fermi levels of the two contacts drives the current (typified by the electro-thermal conductance) which we calculate using the Landauer transport equation. The current shows an initial rise when the device is operated at lower temperatures. The rise stalls at progressively higher temperatures and I_{th} acquires a plateau-like flat profile indicating a competing effect between a larger number of transmission modes and a corresponding drop in the Fermi level difference between the contacts. The current is computed for both *n*- and *p*-type BP and the difference thereof is attributed to the particle-hole asymmetry. We conclude by pointing out improved thermal behaviour that may arise in multi-layered BP through topological phase transitions induced by additional *K*-doping.**

***Index Terms*—Black phosphorus, Seebeck coefficient, Topological transition**

I. Introduction

The miniaturization of circuit components introduces the problem of localized heating that can give rise to temperature overshoots and degrade their overall life span necessitating the need for improved cooling schemes to hold the operating temperature to reasonable limits. While the generated heat can be simply removed, a profitable spin-off is to transform the heat current into electric power taking advantage of the Seebeck effect. This constitutes the basis for electric-thermal energy conversion. The optimization of Seebeck-based power conversion techniques, of late, have received much attention as newer materials [1], notably graphene, hold promise of better thermoelectric operation demonstrated by a higher figure of merit, *ZT*. Black phosphorus (BP), a layered two-dimensional (2D) material [2], [3] offers a viable alternative [4]–[6] to existing thermoelectric materials with a *ZT* predicted to touch 2.5. This large *ZT* has been attributed, in part, to the intrinsic anisotropy [7] of BP. More recently, a highly anisotropic form of BP was found by Kim *et al.* ; they showed that a four-layered BP slab, the armchair (*y*-axis) direction carried a linear dispersion while acquiring a parabolic character along the zigzagged *x*-axis, effectively a semi-Dirac system. Further, doping with potassium (K) allowed a tuning and eventual closing of the band gap and a transition from normal to topological insulating behaviour. We examine a thermally-driven current (I_{th}) in semi-Dirac BP that flows on account of temperature (T) gradient created difference in Fermi distribution (f) at the contacts (Fig. 1). Further, following the findings of Kim *et al.* , who uncovered a subsequent transition from semi-Dirac to linearly dispersing topological states with enhanced *K*-doping, carry out a comparison of the aforementioned thermal currents in prototype linear and parabolic materials. Primarily, we find that the thermal current which flows on application of a temperature gradient is highest in semiconductors which can be grouped as semi-Dirac materials, followed by gapped graphene-like systems with Dirac dispersion, and conventional parabolic conduction bands.

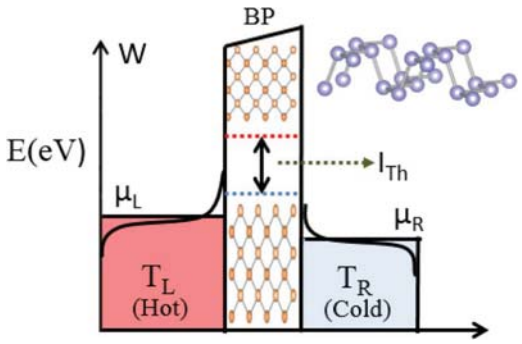

Fig. 1. The schematic illustrates the suggested arrangement of a BP channel flanked between left and right contacts maintained at temperatures $T_L > T_R$ and electrochemical potentials μ_L and μ_R, respectively. The curved lines denote the smeared Fermi function at a finite temperature. A thermally-excited electron (hole) current (I_{th}) flows from the contact at a higher (lower) temperature. The inset shows the puckered unit cell of a single layer BP. The channel dimensions (in appropriate units) are L and W along the *x*- and *y*-axes.

II. Materials and Methods

A semi-Dirac material [8] is characterized by a set of parabolic and linear bands along two mutually perpendicular directions. The minimal Hamiltonian is

$$\mathcal{H} = \left(\Delta + \alpha k_x^2\right)\tau_x + \beta k_y \tau_y. \quad (1)$$

In Eq. 1, the coefficient $\alpha = \hbar^2/2m_e$ and $\beta = \hbar v_f$. The Fermi velocity is v_f, the effective mass is m_e, and $\tau_{x,y}$ represent the iso-spin matrices. For a generalized case, we also include a

978-1-5386-6790-3/18/$31.00 ©2018 IEEE

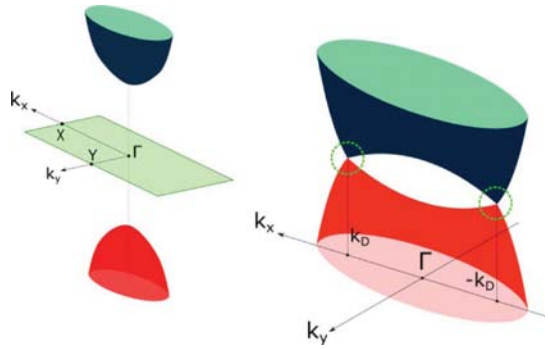

Fig. 2. The schematic depiction (left figure) of the dispersion of a semi-Dirac gapped four-layered BP slab. For the semi-Dirac case, the linear dispersion is along the *y*-axis while the *x*-axis hosts a conventional parabolic band. The band gap closing (right figure) happens when BP is doped with potassium (*K*) and the dopant density reaches a threshold value. The band gap closing at non points is shown by dotted circles. The dopant (*K*) induces an electric field which modulates the band gap. As an illustration of a multi-layered structure, four BP sheets stacked together along an out-of-plane axis (inter-layer spacing is $5.3\,\mathring{A}$) give rise to a semi-Dirac dispersion with a finite gap adjustable through *K*-doping. The single-layer BP is actually a double layered structure and has two P-P bonds. The shorter bond (bond length is $2.22\,\mathring{A}$) connects the nearest P atoms in the same plane while the longer bond ($2.24\,\mathring{A}$) connects atoms located in the top and bottom layers of the unit cell.

band gap (Δ) in conjunction with the parabolic set of bands. The dispersion is straightforward to obtain, we have

$$E(k) = \pm\sqrt{\left(\Delta + \alpha k_x^2\right)^2 + \left(\beta k_y\right)^2}. \tag{2}$$

The + (-) sign in the energy expressions denote the conduction (valence) state. The dispersion by letting $\Delta \to 0$ in Eq. 2 clearly points to mass-less Dirac Fermions along the armchair direction (*y*-axis) while the zigzag axis (*x*-axis) hosts the conventional 'massive' parabolic electron. The band gap in Eq. 2 is tunable in case of BP through *K*-doping which vanishes at a threshold value. The above dispersion relation which holds true for a four-layered BP (adequately *K*-doped such that the band gap vanishes) is plotted in Fig. 2 with material parameters in the accompanying caption.

The thermal current that flows between the two contacts is obtained using the Landauer-Büttiker formalism (LBF). [9] For each spin component (assuming the bands are spin-split when BP is grown on a ferromagnetic substrate), it is:

$$I_{th} = \frac{e}{h}\int_{\mathcal{R}} dE\mathcal{M}(E)\,\mathcal{T}(E)\left(f_L(E,T_L) - f_R(E,T_R)\right). \tag{3}$$

The transmission probability in Eq. 3, for an electron to traverse the channel length (the longitudinal dimension) is $\mathcal{T}(E)$, the function $\mathcal{M}(E)$ is the number of modes, and $f_{L,R}(E,T_{L,R})$ represents the Fermi distribution at the two contacts. As a first approximation, we set the transmission to unity assuming the target structure (see Fig. 1) to be homogeneous throughout. To estimate $\mathcal{M}(E)$, as is standard practice, we assume periodic boundary conditions along the *y*-axis such that the k-channels are equi-spaced by $2\pi/W$. [10], [11] Here, W is the width (the transverse span along the *y*-axis) of the sample. Each unique k-vector is a distinct mode and the number of such momentum vectors is determined from the inequality, $-k_f < k_y < k_f$. The upper and lower bounds of the inequality are the momentum vectors that correspond to the Fermi energy, E_f. The approximate number of modes is therefore $k_f W/\pi$. Also, note that the integral in Eq. 3 must be evaluated over two energy-manifolds, each in the vicinity of the conduction (E_c) and valence band (E_v) extremum. Explicitly, the energy manifold of integration (Eq. 3) is a simple union of two disjoint intervals given by $\mathcal{R}_1 : E \in \{-\infty, E_v\}$ and $\mathcal{R}_2 : E \in \{E_c, \infty\}$. The domain is then, $\mathcal{R} = \mathcal{R}_1 \cup \mathcal{R}_2$. Bearing these in mind, Eq. 3 for thermal current can be recast as

$$I_{th} = \frac{eW}{\pi h}\int_{\mathcal{R}} g(E)\,dE\int_{-\pi/2}^{\pi/2} d\theta\cos\theta\left(f_1(T_1) - f_2(T_2)\right). \tag{4}$$

The function $g(E)$ in Eq. 4 is the analytic representation of the k-vector in energy space. Using Eq. 2 and the exchange field, the function $g(E)$ is

$$g(E) = \left[\frac{1}{2\alpha^2\cos^4\theta}\left(\Omega - \left(2\alpha\Delta\cos^2\theta + \beta^2\sin^2\theta\right)\right)\right]^{0.5}. \tag{5}$$

For brevity, we have used the short-hand notation $\Omega = \sqrt{\left(2\alpha\Delta\cos^2\theta + \beta^2\sin^2\theta\right)^2 + 4\cos^4\theta\left(\mathcal{E}^2 - \Delta^2\right)\alpha^2}$ and $\mathcal{E} = (E - \eta\Delta^{ex})$. As a clarifying note, the sum of modes along the width (W) is $\sum_{k_f W/\pi}\Delta k_y$ which in the continuum limit changes to $\int_{-k_f}^{k_f} dk_y$. As usual, the azimuthal angle is θ while $k_x = k\cos\theta$ and $k_y = k\sin\theta$. Note that the limits of angular integration satisfies the span of a given k-vector $(-k_f < k_y < k_f)$ or mode. To obtain an estimate of the thermal current, a numerical integration of Eq. 4 can be carried out. It is worthwhile to emphasize again on what we briefly alluded to above: The current in Eq. 4 has two components - from the conduction band electrons and the valence band holes - that flow in opposite directions for a certain potential drop. To further elucidate, when the left contact (in Fig. 1) is at a higher temperature than its right counterpart on the right, we define the electron current to flow from the left and empty in the right contact while the hole current flows in the exact opposite sense.

The function $g(E)$ in Eq. 4 changes representation for linear and parabolic bands - two material types that we also consider here. The conventional parabolic (*P*) is expressed as $E_P = \alpha k^2 + \Delta$, where $\alpha = \hbar^2/2m^*$ while the linear Dirac (*L*) is simply $E_L = \sqrt{(\beta k)^2 + \Delta^2}$. The effective mass is m^* and $v_f = \beta/\hbar$ is the Fermi velocity. For completeness, a band gap, Δ, has been added to both dispersion forms. The function $g(E)$ in Eq. 4 for the two cases (*P* & *L*) can therefore be straightforwardly written as:

$$g_P(E) = \sqrt{\frac{1}{\alpha}(E - \Delta)}, \tag{6a}$$

and

$$g_L(E) = \sqrt{\frac{1}{\beta^2}(E^2 - \Delta^2)}. \tag{6b}$$

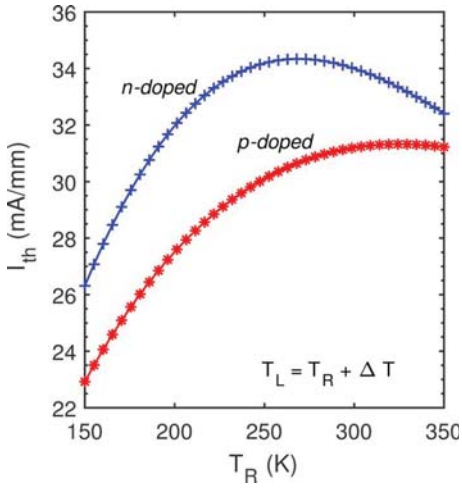

Fig. 3. The numerically obtained current (I) that flows in a multi-layer BP sheet clamped between two contacts at dissimilar temperatures (see Fig. 1) is shown. Mirroring the magnetization-induced asymmetry of the conduction and hole states, I is lower for a *p*-doped material vis-á-vis an *n*-type structure. Note that the temperature (T_R) shown along the *x*-axis is for the left contact; the left contact is always set to $T_R + \Delta T$. Here, $\Delta T = 25\,K$.

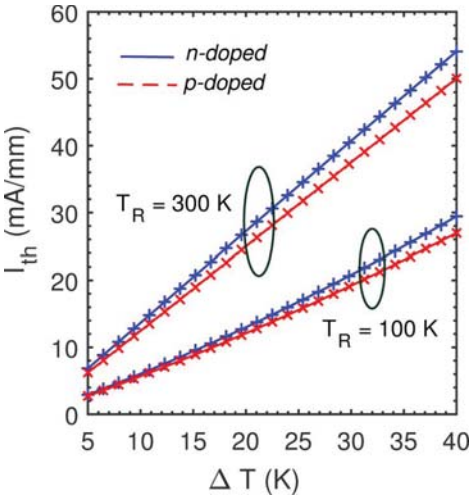

Fig. 4. The thermal current behaviour as a function of temperature difference that exists between the two contacts. The material parameters are identical to those used in Fig. 3. The two temperatures $(T_R = 100, 300\,K)$ indicated on the plot are the starting values for the right contact, the temperature of the left contact $(T_L = T_R + \Delta T)$ is then swept up to enlarge the difference (shown on the *x*-axis) with its right counterpart that progressively enhances the Fermi drop $(\Delta\mu)$ and consequently manifests as a larger thermal current.

III. Numerical Results

The preceding formalism allows us to numerically estimate the quantum of thermal current; to do so, we begin by fixing the parameters starting with the temperatures of the two contacts. The temperature is swept between $T \in [150, 350]\ K$ maintaining a constant difference of $\Delta T = 25\,K$ between the left (hotter) and right contact. The exchange field of the ferromagnet that breaks the particle-hole symmetry is set to $\Delta_{ex} = 30.0\,meV$. As for BP, from previously determined material constants, the effective mass for the parabolic branch is $m_{eff} = 1.42 m_0$ while the band gap with *K*-doping is approximately $\Delta = 0.36\,eV$. The BP band gap is tunable via the concentration of the *K*-dopant. [12] The Fermi velocity for the linear branch is $v_f = 5.6 \times 10^5\,ms^{-1}$. Note that the out-of-plane magnetization splits the conduction and valence bands into spin-up and spin-down ensembles; for the selected material constants, the bottom the conduction spin-up (down) band is $0.21\,(0.15)$ eV. The corresponding top of the spin-up (down) valence band is $-0.15\,(-0.21)\ eV$. The Fermi distribution functions (see Eq. 4) are computed by assigning an identical electrochemical potential (μ) to both contacts; to simulate *n*- and *p*-type character, we toggle μ between $\pm 0.17\,eV$. In each case, μ is located between the bottom (top) of the spin-split conduction (valence) spin-up and spin-down bands. The current (see Fig. 3) is obtained by a numerical integration (Eq. 4) considering all possible modes within $65.0\,meV$ from the conduction and valence band extremum and a range of temperatures while holding a constant difference between the contacts.

We comment on a few noteworthy features of Fig. 3; firstly, it is immediately recognizable that as the temperature rises, the thermal current begins to saturate for both *n*- and *p*-type, a behaviour attributable to the diminishing Fermi level difference $(\Delta\mu)$ with a rise in temperature for a given energy. At hand though, there also exists a larger smearing of the Fermi function at a higher temperature opening up additional modes $((M)$ in Eq. 4) accessible for transport, however, in this case, the fall in $\Delta\mu$ executes the more definitive role. In the same spirit, for a fixed temperature, the current falls (see inset, Fig. 3) at higher energies as $\Delta\mu$ is again lowered for a pre-determined temperature difference between the contacts. To offer additional substantiation to this line of reasoning, a plot (Fig. 4) of the thermal current for several temperatures differences is distinguished by an increasing behaviour, a fact that constitutes a simple demonstration of an enlarged $\Delta\mu$. This increment to $\Delta\mu$ translates into a higher current. Notice that the current (for both doping cases) shown in Fig. 3 receives contribution from four components: They are a pair consisting of spin-up and spin-down electron components from the conduction bands and a similar but counteracting hole-based set originating in the valence bands. When BP is doped *n*-type, the position of the Fermi level in the conduction band guarantees completely (almost, if smearing is accounted) filled valence bands, a consequence of which is a negligible hole current. By the same token, for a *p*-type material, the conduction states are nearly empty ensuring that bulk of the current is carried by holes. From an experimental standpoint, both *n*- and *p*-type conduction has been observed [13] in BP consistent with the narrow band gap that permits tuning of the Fermi level close to either the valence or conduction band.

For a similar exercise with the parabolic material, the effective mass is set to $0.0565 m_0$, where $m_0 = 9.1 \times 10^{-31} kg$ is the free electron mass. In practice, this corresponds to the transverse mass of conduction electrons located at the L-valley of a $6.0\,nm$ wide PbTe thin film, which is modeled as a quantum well. The choice of PbTe [14], [15] is is motivated by its wide applicability in the design of thermoelectric devices. The direct L-valley band gap (Δ_P) at such temperatures for

PbTe can be set [16] to $0.19eV$. The linear counterpart is chosen to be graphene grown on a substrate that gaps the Dirac cones at the K and $K^{'}$ edges of the Brillouin zone. A large number of substrates have been investigated that lower the C_{6v} point group symmetry of pristine graphene to C_{3v} introducing a band gap and turning it into a semiconductor; the chief candidates being hexagonal boron nitride (h-BN), silicon carbide (SiC), and oxides such as Al_2O_3 and MgO. As a case in point and which serves our goal well by virtue of a more accurate comparison between parabolic and linear materials, graphene grown on Al-terminated Al_2O_3 surface is predicted to have a band gap of $0.18\,eV$, a number closely aligned to the $0.19\,eV$ adopted for representative parabolic PbTe. In light of this brief note, we set the linear band gap (Δ_L) equal to its parabolic counterpart $(\Delta = \Delta_L = \Delta_P)$, which is $0.19\,eV$. The current that flows in the setup of Fig. 1 only under a temperature gradient is compared in Fig. 5 for linear and parabolic materials for a series of externally adjusted temperatures (T_R) of the right contact. The Fermi level for both class of materials was set to the bottom of the conduction band and an energy window of $65\,meV$ was assumed for the numerical integration of Eq. 4. The temperature difference between the contacts $(T_L - T_R)$ was fixed to $25\,K$. As for the choice of energy levels, we adopt the following reference levels: The bottom of the conduction band (CB) for the parabolic material is identical to the band gap (Δ), and therefore the top of the valence band (VB) is zero. The semi-metal graphene (with both CB and VB equi-energetic at $0\,eV$) when gapped by a substrate symmetrically splits the CB and VB bands; the bottom of the CB is located at $\Delta/2$ and top of the VB is pushed down to -$\Delta/2$.

IV. Concluding remarks

We have predicted the quantum of thermally-driven current in a semi-Dirac multi-layered BP slab held between contacts at different temperatures. The presented results serve not just as an illustration of the microscale thermal-to-electric energy 'harvesting' paradigm [17] via a Seebeck-like power generator but also emphasize on the greater efficiency of the semi-Dirac nature of BP in designing advanced thermal management schemes enhancing the lifetime and reliability of microchips. The experimental challenge in constructing such thermal converters lies in controlling the temperature gradient, since the heat current tends to delocalize over the channel length. Lastly, notice that the set up described here is essentially a formulation of the Seebeck phenomenon or the production of thermopower, which in case of BP, can be modulated through a variety of means by pursuing the standard route [18] of density-of-states (DOS) calibration. One such technique involves the application of an intense light beam [19] and the attendant changes to the band dispersion and DOS.

Briefly, it is relevant to state here that BP which turns semi-Dirac with *K*-doping can undergo a topological phase transition with increasing dopant concentration through a vanishing of the band gap. Beyond the band gap ceasing, for a higher

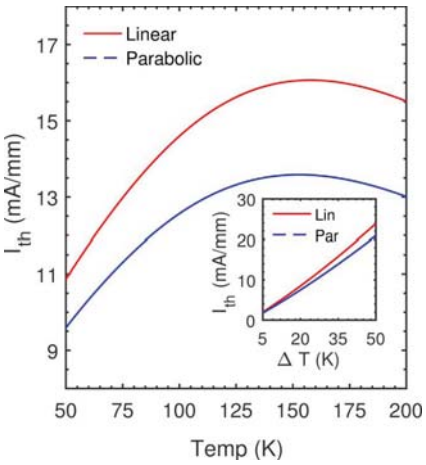

Fig. 5. The numerically calculated thermal current for a fixed temperature difference (ΔT) between the contacts (see Fig. 1) when linear and parabolic materials are used is shown on the right panel (b). For calculation/numerical parameters described in the text, the linear material offers a greater quantum of thermal current in comparison to the parabolic case, attributable to a higher density of states in the former. Note that the current flows because of a temperature difference induced inequality in the Fermi level of the contacts. The numbers on the *x*-axis indicate the temperature of the right contact (T_R); the left contact temperature (T_L) for this plot is therefore $T_L = T_R + \Delta T$. As further evidence of this point, the inset plot shows current as a function of (ΔT) between the contacts; a higher difference is reflected in a rising thermal current. Specifically, $T_R = 50\,K$ and T_L as before is higher by (ΔT). Note that no net current actually flows (unless the circuit is completed via connectors) and only an open circuit voltage is measured as shown by the left panel schematic (a). In an open circuit case (vanishing net current), the initial response to ΔT is a diffusion current which is exactly counteracted by a internal drift component set up by an electric field oppositely directed to the temperature gradient vector.

K-dopant concentration, paves the way for band inversion, a precursor to topologically protected states; indeed, such states with massless and anisotropic Dirac fermions [12] have been observed in BP. A simplified form of the Hamiltonian for the topological insulator (TI) can be written as

$$\mathcal{H}_{TI} = \hbar\, v_x\, (k_x - k_D)\, \sigma_x + \hbar\, v_y k_y \sigma_y, \tag{7}$$

where v_x and v_y are the velocities along the *x*- and *y*-axes, respectively at the Dirac point. A Dirac graphene-like dispersion (Eq. 7)is characterized by a DOS that linearly scales with $|\epsilon|$ and may therefore exhibit (for a finite energy) a larger heat capacity in comparison to a semi-Dirac or parabolic 2D nanostructure. It is decidedly an attractive proposition to observe topological phase transitions via doping and the concurrent advantages [20] that accrue; however, the benefits of the strong anisotropy of BP, particularly suited for a large ZT may disappear. A careful set of experimental measurements may uncover the precise connection between topological phase transitions and the overall thermoelectric behaviour in semi-Dirac BP.

References

[1] A. Minnich, M. Dresselhaus, Z. Ren, and G. Chen, "Bulk nanostructured thermoelectric materials: current research and future prospects," *Energy & Environmental Science*, vol. 2, no. 5, pp. 466–479, 2009.

[2] X. Ling, H. Wang, S. Huang, F. Xia, and M. S. Dresselhaus, "The renaissance of black phosphorus," *Proceedings of the National Academy of Sciences*, vol. 112, no. 15, pp. 4523–4530, 2015.

[3] H. Liu, Y. Du, Y. Deng, and D. Y. Peide, "Semiconducting black phosphorus: synthesis, transport properties and electronic applications," *Chemical Society Reviews*, vol. 44, no. 9, pp. 2732–2743, 2015.
[4] H. Lv, W. Lu, D. Shao, and Y. Sun, "Large thermoelectric power factors in black phosphorus and phosphorene," *arXiv preprint arXiv:1404.5171*, 2014.
[5] Y. Saito, T. Iizuka, T. Koretsune, R. Arita, S. Shimizu, and Y. Iwasa, "Gate-tuned thermoelectric power in black phosphorus," *Nano Letters*, vol. 16, no. 8, pp. 4819–4824, 2016.
[6] J. Zhang, H. Liu, L. Cheng, J. Wei, J. Liang, D. Fan, J. Shi, X. Tang, and Q. Zhang, "Phosphorene nanoribbon as a promising candidate for thermoelectric applications," *Scientific reports*, vol. 4, p. 6452, 2014.
[7] R. Fei, A. Faghaninia, R. Soklaski, J. Yan, C. Lo, and L. Yang, "Enhanced thermoelectric efficiency via orthogonal electrical and thermal conductances in phosphorene." *Nano letters*, vol. 14, no. 11, p. 6393, 2014.
[8] S. Banerjee and W. E. Pickett, "Phenomenology of a semi-dirac semi-weyl semimetal," *Physical Review B*, vol. 86, no. 7, p. 075124, 2012.
[9] Z. P. Niu, Y. M. Zhang, and S. Dong, "Enhanced valley-resolved thermoelectric transport in a magnetic silicene superlattice," *New Journal of Physics*, vol. 17, no. 7, p. 073026, 2015.
[10] S. Datta, *Electronic transport in mesoscopic systems*. Cambridge university press, 1997.
[11] A. D. Stone and A. Szafer, "What is measured when you measure a resistance?the landauer formula revisited," *IBM Journal of Research and Development*, vol. 32, no. 3, pp. 384–413, 1988.
[12] S. Baik, K. Kim, Y. Yi, and H. Choi, "Emergence of two-dimensional massless dirac fermions, chiral pseudospins, and berry's phase in potassium doped few-layer black phosphorus." *Nano letters*, vol. 15, no. 12, p. 7788, 2015.
[13] L. Li, Y. Yu, G. J. Ye, Q. Ge, X. Ou, H. Wu, D. Feng, X. H. Chen, and Y. Zhang, "Black phosphorus field-effect transistors," *Nature nanotechnology*, vol. 9, no. 5, pp. 372–377, 2014.
[14] P. Sengupta, Y. Wen, and J. Shi, "Spin-dependent magneto-thermopower of narrow-gap lead chalcogenide quantum wells," *Scientific reports*, vol. 8, no. 1, p. 5972, 2018.
[15] P. Sengupta and J. Shi, "Rashba-driven anomalous nernst conductivity of high spin-orbit-coupled lead chalcogenide films," *Physical Review Materials*, vol. 2, no. 6, p. 064606, 2018.
[16] G. Foley and D. Langenberg, "Electronic structure of pbte near the band gap," *Physical Review B*, vol. 15, no. 10, p. 4850, 1977.
[17] X. Zhang and L.-D. Zhao, "Thermoelectric materials: energy conversion between heat and electricity," *Journal of Materiomics*, vol. 1, no. 2, pp. 92–105, 2015.
[18] M. Jonson and G. Mahan, "Mott's formula for the thermopower and the wiedemann-franz law," *Physical Review B*, vol. 21, no. 10, p. 4223, 1980.
[19] P. Sengupta and S. Rakheja, "Anisotropy-driven quantum capacitance in multi-layered black phosphorus," *Applied Physics Letters*, vol. 111, no. 16, p. 161902, 2017.
[20] D. J. Perello, S. H. Chae, S. Song, and Y. H. Lee, "High-performance n-type black phosphorus transistors with type control via thickness and contact-metal engineering," *Nature communications*, vol. 6, p. 7809, 2015.